MONTE CARLO STUDY OF MAGNETIC CHARACTERISTICS OF THE DOUBLE PEROVSKITE Sr_2FeMoO_6

I.A. BADROUR, N. HACHEM*, M. EL BOUZIANI

Laboratory L.P.M.C., Faculty of Sciences, Chouaïb Doukkali University, El Jadida, Morocco
Corresponding author*: hachem.n@ucd.ac.ma

Received March 7, 2025

Abstract. Certain magnetic characteristics and the hysteresis behavior of double perovskite Sr_2FeMoO_6 were analysed through Monte Carlo simulation. Our investigation shows this ferrimagnetic compound exhibits a second-order phase transition at a Curie temperature $T_C = 490$ K. The effect of the crystal field on magnetization was examined, and a phase diagram was plotted in the (crystal field, temperature) plane. Furthermore, in the presence of an external magnetic field, the influence of temperature on the hysteresis loop's behaviour was explored.

Key words: Double perovskite Sr_2FeMoO_6; Magnetic properties; Monte Carlo; Curie temperature.

DOI: https://doi.org/10.59277/RomJPhys.2025.70.614

1. INTRODUCTION

The general formula of the double perovskite is $A_2BB'O_6$, where A is an alkaline earth or rare-earth ion, B and B′ are two transition metals, and O is oxygen [1–6]. The most widely investigated of these compounds is Sr_2FeMoO_6 (SFMO), which exhibits ferrimagnetic and semi-metallic characteristics, with high spin polarization at the Fermi level and a Curie temperature higher than room temperature [1–5]. These features make double perovskite SFMO interesting for several technological applications such as magnetic random-access memories, magnetic sensors, spin injectors, and read-write heads [7–9].

The literature describes different synthesis methods for Sr_2FeMoO_6 and also gives numerous results concerning its magnetic properties, such as saturation magnetization, Curie temperature, magnetoresistance, and variation of resistivity with temperature [10, 11]. Some studies on the Fe/Mo order have shown that at low fields, the magnetoresistance and saturation magnetization of SFMO are sensitive to anti-site defects [12, 13]. The presence of oxygen vacancies can increase the Curie temperature and reduce the magnetization in SFMO [14]. From the total energy optimization, SFMO is stable in tetragonal structure [15]. The impact of biaxial mechanical deformation on the magnetic and electronic behaviours of double perovskite SFMO has been investigated by means of density functional theory [16]. Furthermore, the double perovskite SFMO has been produced by solid-state method at low temperatures, where its behaviour is interpreted as a function of ferrimagnetic couplings resulting from the varying distributions of local interactions between neighbouring Fe and Mo atoms [17].

The Monte Carlo simulation (MCS) is a powerful numerical approach for simulating the magnetic behaviour of double perovskite compounds. For this reason, we have opted to use MCS to study certain magnetic properties of Sr_2FeMoO_6, notably the Curie temperature, saturation magnetization, and hysteresis behaviour. The rest of this article is structured as follows: Section 2 presents the model and Monte Carlo method employed to simulate this compound. In Section 3, numerical results concerning the Curie temperature and the impacts of crystal field and temperature on the magnetization and hysteresis behaviour of Sr_2FeMoO_6 are explored and commented. Lastly, our conclusion is given in Section 4.

2. MODEL AND MONTE CARLO METHOD

The double perovskite Sr_2FeMoO_6 has a cubic symmetry with the space group Fm3m (Fig. 1) [18, 19]. Oxygen (O) atoms form octahedra surrounding the sites occupied by iron (Fe) and molybdenum (Mo) atoms. The MoO_6 and FeO_6 octahedra are ordered by a three-dimensional alternation; each MoO_6 octahedron has only FeO_6 octahedra as neighbours and *vice versa*. Strontium (Sr) atoms are located in the hollow sites formed by the vertices of the MoO_6 and FeO_6 octahedra. In reality, under the effect of temperature and pressure, the SFMO unit-cell structure is quadratic and belongs to the space group I4/mmm, with slight distortion along the $z-$axis and lattice parameters: $a = 5.58$Å and $c = 7.90$ Å [20].

The magnetic atoms Fe and Mo in Sr_2FeMoO_6 constitute two interpenetrating sublattices (A) and (B) with spins $S = 5/2$ and $\sigma = 1/2$, respectively [1, 2]. In this work, the SFMO compound is described within an Ising-type model by the following Hamiltonian:

$$H = -J_{AB}\sum_{\langle ij\rangle} S_i\sigma_j - J_A\sum_{\langle ik\rangle} S_iS_k - J_B\sum_{\langle jm\rangle}\sigma_j\sigma_m - D\sum_i S_i^2 - h\left(\sum_i S_i + \sum_j \sigma_j\right) \tag{1}$$

where the spins S_i can assume the values $\pm5/2$, $\pm3/2$, and $\pm1/2$, and the spins σ_j can assume the values $\pm1/2$. J_{AB}, J_A, and J_B represent the exchange interaction constants between nearest-neighbour spins $S-\sigma$, $S-S$, and $\sigma-\sigma$, respectively. Since Sr_2FeMoO_6 is ferrimagnetic, we consider: $J_{AB} < 0$, $J_A > 0$, and $J_B > 0$. D is the crystal field acting on spins $S = 5/2$, and h is the applied magnetic field acting on all spins.

To simulate the system's Hamiltonian H, we employed the standard Monte Carlo technique based on the metropolis algorithm [21] and applied it to a cubic

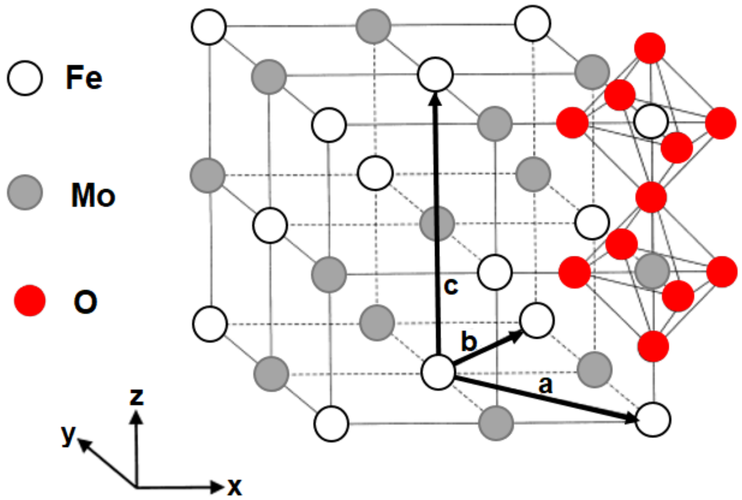

Fig. 1 – Crystal structure of double perovskite Sr_2FeMoO_6, with Sr atoms omitted and a selection of O atoms displayed.

lattice of side $L = 30$. Beginning with an initial random spin configuration, new configurations are formed by inverting spins, which are either accepted or discarded on the basis of a probability determined by Boltzmann statistics. The means of various physical quantities are computed *via* 10^5 Monte Carlo steps per site, following the exclusion of the initial 2.10^4 steps per site to ensure system equilibration. Among these quantities, our program is able to compute:

• The magnetizations per site m_A and m_B of Fe-sublattice (A) and Mo-sublattice (B), respectively, containing N_{Fe} and N_{Mo} spins:

$$m_A = \frac{1}{N_{Fe}} \sum_{i=1}^{N_{Fe}} S_i \qquad \text{and} \qquad m_B = \frac{1}{N_{Mo}} \sum_{j=1}^{N_{Mo}} \sigma_j \tag{2}$$

• The total magnetization per site M:

$$M = \frac{(N_{Fe} \times m_A) + (N_{Mo} \times m_B)}{N} \tag{3}$$

• The total magnetic susceptibility per site χ:

$$\chi = \beta\, N \left(\langle M^2 \rangle - \langle M \rangle^2 \right) \tag{4}$$

where $\beta = 1/(k_B T)$, with T representing the absolute temperature and k_B denoting the Boltzmann constant. Here, k_B is considered to be equal to unity ($k_B = 1$). $N = L \times L \times L = 30 \times 30 \times 30$ stands for the total number of spins in the lattice, and $N_{Fe} = N/2$ and $N_{Mo} = N/2$ are the numbers of spins in sublattices (A) and (B), respectively.

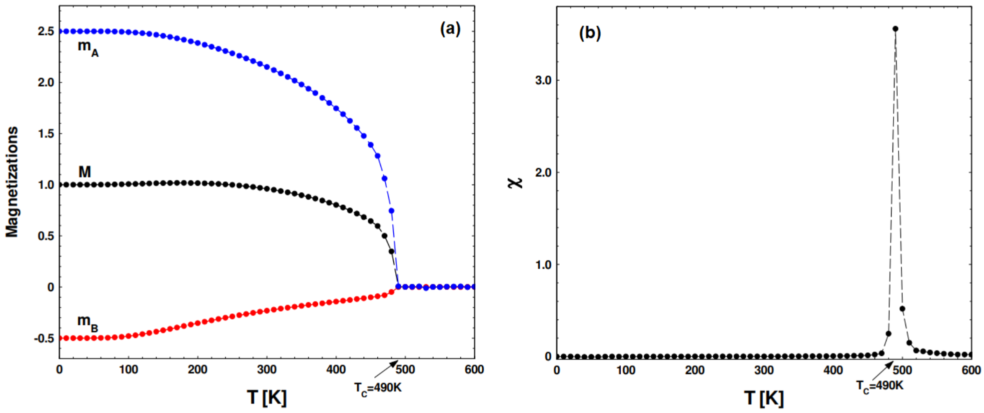

Fig. 2 – Magnetizations m_A, m_B, and M (a) and total susceptibility χ (b) as a function of temperature in the compound Sr_2FeMoO_6, for $J_{AB} = 20K$, $J_A = 17K$, and $J_B = 16K$.

3. MAGNETIC PROPERTIES AND HYSTERESIS BEHAVIOR

First, we aim to determine the Curie temperature T_C, where the ferrimagnetic-paramagnetic phase transition takes place in the double perovskite Sr_2FeMoO_6. Figure 2(a) shows the variation with temperature of the magnetizations m_A, m_B, and M, for the same values of exchange interactions obtained for the stable system configuration by *ab initio* calculations in Refs. [11, 22]: $|J_{AB}| = |J_{Fe-Mo}| = 20K$, $J_A = J_{Fe-Fe} = 17K$, and $J_B = J_{Mo-Mo} = 16K$. It can be seen that the saturation values of the magnetizations m_A, m_B, and M at $T = 0K$ are 2.5, -0.5, and 1, respectively. By increasing temperature, the three magnetizations vary continuously (m_A and M decrease, while m_B increases) up to zero at $T_C = 490K$. In Fig. 2(b), the magnetic susceptibility χ confirms the value of the critical temperature found, peaking at $T_C = 490K$. This value of T_C is comparable to those between $410 - 450K$, found in previous studies [1, 2, 10, 18, 23–25]. Obtaining a high T_C makes Sr_2FeMoO_6 a very attractive candidate for magnetocaloric applications [25].

In what follows, for simplicity's sake, we consider J_{AB} as a unit of energy and temperature, *i.e.*, $J_{AB} = -1$, $J_A = 0.85$, and $J_B = 0.8$. The impact of the crystal field D on the critical and magnetic behaviours of the compound Sr_2FeMoO_6 is examined in Fig. 3, where we present the thermal variations of the magnetizations m_A and m_B (Fig. 3(a)), and M (Fig. 3(b)), for several chosen values of D and $h = 0$. It is worth pointing out that it is not easy to change the crystal field in materials, but this can be achieved through the application of external stimuli like pressure or light irradiation [26]. Figure 3(a) illustrates that the saturation value of the magnetization per site of the Fe-sublattice (A) can take one of three values: 2.5, 1.5, and 0.5, which decreases as $|D|$ increases. Indeed, the low-spin and high-spin states are influenced by the strength of the crystal field; strong crystal fields favour the low-spin state, whereas

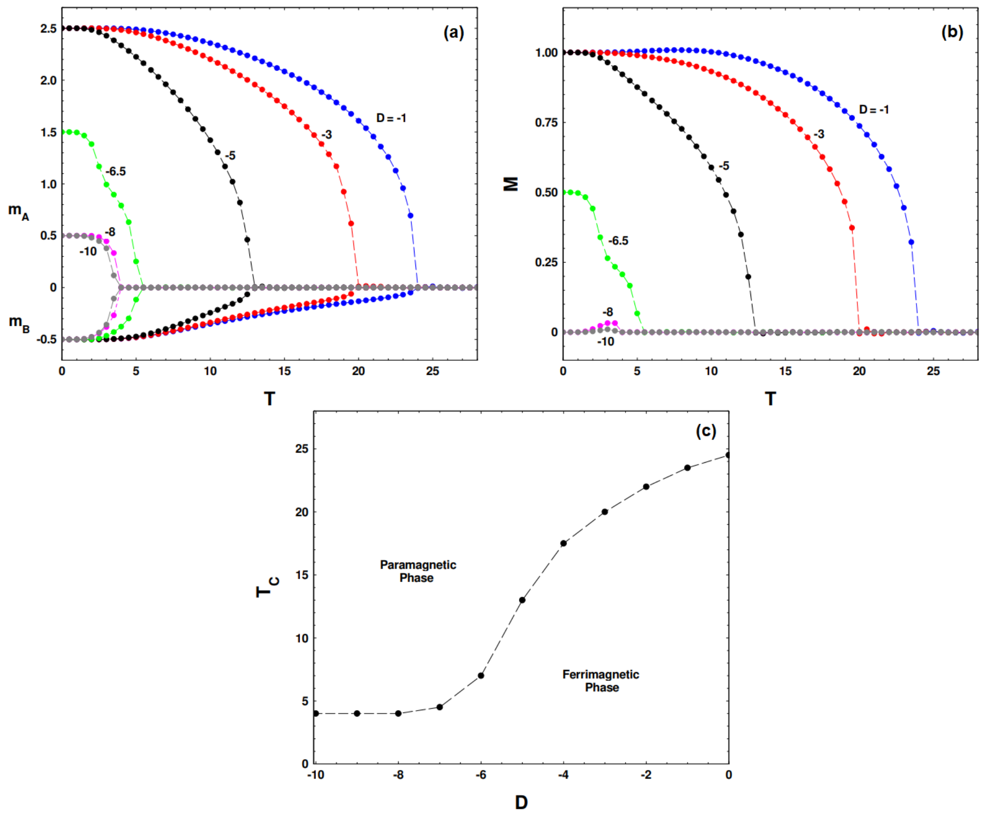

Fig. 3 – Thermal variations of magnetizations (a) m_A and m_B, and (b) M for chosen values of D, and (c) phase diagram in the (D, T) plane, when $J_{AB} = 1$, $J_A = 0.85$, $J_B = 0.8$, and $h = 0$.

weak crystal fields favour the high-spin state [27]. Furthermore, the magnetization per site of the Mo-sublattice (B) has a unique saturation value of -0.5, whatever the value of D. Thus, the total magnetization per site M exhibits three saturation values: 1, 0.5, and 0, decreasing with increasing $|D|$, as seen in Fig 3(b). With increasing temperature, the magnetizations m_A and M exhibit a continuous decrease, whereas the magnetization m_B shows a continuous increase. These trends persist until all three magnetizations cancel out at a critical temperature T_C that decreases with rising $|D|$. After identifying the T_C for various values of D, we constructed the phase diagram of the double perovskite SFMO in the (D, T) plane in Fig. 3(c), with $h = 0$. It is clear that for all crystal field values, a paramagnetic phase exists at high temperatures and a ferrimagnetic phase at low temperatures, separated by a second-order phase transition at T_C. The latter decreases as $|D|$ increases, eventually reaching a constant value ($T_C = 4$) when D becomes sufficiently large. Similar critical and magnetic behaviours were reported in systems with mixed spin-$1/2$ and spin-$5/2$ configurations

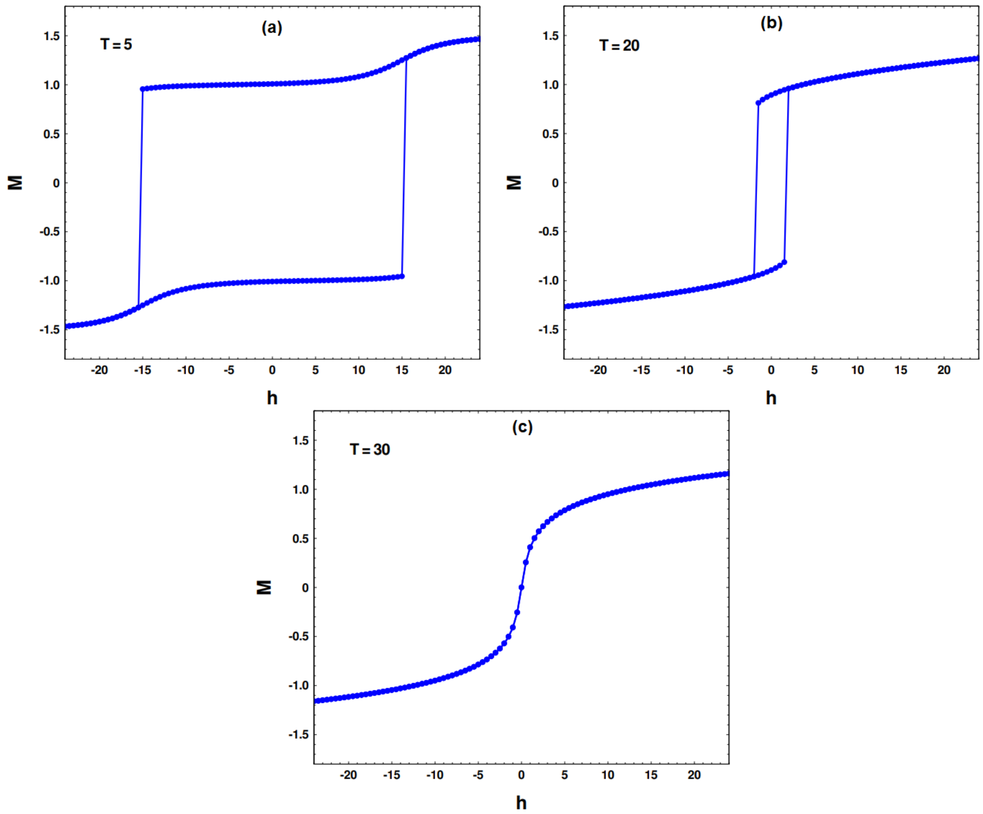

Fig. 4 – Hysteresis loops for chosen values of temperature: (a) $T = 5$, (b) $T = 20$, and (c) $T = 30$, when $J_{AB} = -1$, $J_A = 0.85$, $J_B = 0.8$, and $D = 0$.

using theoretical approaches [28–31].

Let us now explore the impact of the external magnetic field ($h \neq 0$) and analyse how temperature influences the hysteresis behaviour of the material. Figure 4 illustrates the dependence of total magnetization per site M on h at different temperatures, when $J_{AB} = -1$, $J_A = 0.85$, $J_B = 0.8$, and $D = 0$. As T increases from 0 to higher values, the hysteresis loop area, remanent magnetization, and coercive field gradually diminish, ultimately leading to the complete disappearance of the loop. For low temperatures, as for $T = 5$ in Fig. 4(a), the material features a large hysteresis loop. Then, as T increases, the loop shrinks and narrows, as observed for $T = 20$ in Fig. 4(b). Eventually, at high temperatures exceeding the critical temperature $T_C = 24.5$, the hysteresis loop vanishes entirely, as for $T = 30$ in Fig. 4(c), indicating that the compound becomes completely paramagnetic. This finding aligns with the results achieved in earlier studies on double perovskite Sr_2FeMoO_6 [1, 11, 25].

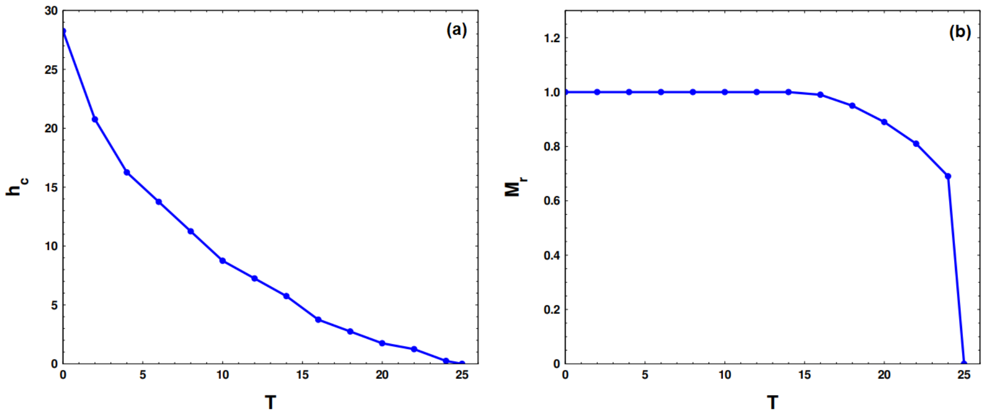

Fig. 5 – Variation of the coercivity h_c (a) and remanence M_r (b) as a function of temperature T, when $J_{AB} = -1$, $J_A = 0.85$, $J_B = 0.8$, and $D = 0$.

To further discuss the influence of temperature on the coercivity h_c and remanence M_r of this compound, we show the thermal variations of these two hysteretic parameters in Fig. 5, for $J_{AB} = -1$, $J_A = 0.85$, $J_B = 0.8$, and $D = 0$. From Fig. 5(a), we can see that h_c gradually decreases as T increases until it is cancelled. However, in Fig. 5(b), M_r remains constant at low temperatures ($M_r = 1$), and as T rises above value 15, M_r begins to decrease rapidly until it disappears. These behaviours of h_c and M_r under the impact of temperature are similar to those obtained for other double perovskites, such as Ca_2FeReO_6 [32] and $Ba_{1.7}La_{0.3}FeMoO_6$ [33].

4. CONCLUSION

Using Monte Carlo simulation, we have explored some of the magnetic characteristics and hysteresis behaviour of double perovskite Sr_2FeMoO_6. We have determined the Curie temperature for this compound ($T_C = 490K$), which closely matches the values reported in experimental studies. The analysis of the impact of crystal field D on magnetization indicates that the negative increase in this field reduces the Curie temperature, reaching saturation for large values of $|D|$. A phase diagram plotted in the (crystal field, temperature) plane reveals the existence of a second-order phase transition line, separating a ferrimagnetic phase at low temperatures from a paramagnetic one at high temperatures. Additionally, by applying a magnetic field, we have examined the hysteresis loop's behaviour as a function of temperature. The material displays a hysteresis loop that gradually shrinks and narrows as the temperature rises, eventually vanishing completely.

REFERENCES

1. K.I. Kobayashi, T. Kimura, H. Sawada, K. Tekura, Y. Tokura, Nature **395**, 677 (1998).
2. A.S. Ogale, S.B. Ogale, R. Ramesh, T. Venkatesan, Appl. Phys. Lett. **75**, 537 (1999).
3. D.D. Sarma, P. Mahadevan, T. Saha-Dasgupta, S. Ray, A. Kumar, Phys. Rev. Lett. **85**, 2549 (2000).
4. Z. Szotek, W.M. Temmerman, A. Svane, L. Petit, H. Winter, Phys. Rev. B **68**, 104411 (2003).
5. C. Frontera, J. Fontcuberta, Phys. Rev. B **69**, 014406 (2004).
6. E. Burzo, I. Balasz-Muresan, Rom. J. Phys. **62**, 601 (2017).
7. Y. Moritomo, S. Xu, A. Machida, T. Akimoto, E. Nishibori, M. Takata, M. Sakata, Phys. Rev. B **61**, R7827 (2000).
8. M. Retuerto, M.J. Martínez-Lope, M. García-Hernández, J.A. Alonso, J. Phys.: Condens. Matter **21**, 186003 (2009).
9. C.W. Yang, T.T. Fang, J. Electrochem. Soc. **159**, 35 (2012).
10. R.P. Borges, R.M. Thomas, C. Cullinan, J.M.D. Coey, R. Suryanarayanan, L. Ben-Dor, L. Pinsard-Gaudart, A. Revcolevschi, J. Phys.: Condens. Matter **11**, L445 (1999).
11. A.S. Erchidi Elyacoubi, R. Masrour, A. Jabar, M. Ellouze, E.K. Hlil, Mater. Res. Bull. **99**, 132 (2018).
12. J. Navarro, L.I. Balcells, F. Sandiumenge, M. Bibes, A. Roig, B. Martínez, J. Fontcuberta, J. Phys.: Condens. Matter **13**, 8481 (2001).
13. X.M. Feng, G.H. Rao, G.Y. Liu, H.F. Yang, W.F. Liu, Z.W. Ouyang, J.K. Liang, Physica B **344**, 21 (2004).
14. M. Hoffmann, V.N. Antonov, L.V. Bekenov, K. Kokko, W. Hergert, A. Ernst, J. Phys.: Condens. Matter **30**, 305801 (2018).
15. S.E.A. Yousif, O.A. Yassin, J. Alloys Compd. **506**, 456 (2010).
16. R. Lu, H. Wu, Y. Qian, E. Kan, Y. Liu, W. Tan, C. Xiao, K. Deng, Solid State Commun. **191**, 70 (2014).
17. C. Bartha, C. Plapcianu, A. Crisan, M. Enculescu, A. Leca, Dig. J. Nanomater. Biostructures **11**, 773 (2016).
18. D. Serrate, J.M. De Teresa, M.R. Ibarra, J. Phys.: Condens. Matter **19**, 023201 (2007).
19. A. Arulraj, K. Ramesha, J. Gopalakrishnan, C.N.R. Rao, J. Solid State Chem. **155**, 233 (2000).
20. S. Colis, D. Stoeffler, C. Mény, T. Fix, C. Leuvrey, G. Pourroy, A. Dinia, P. Panissod, J. Appl. Phys. **98**, 033905 (2005).
21. N. Metropolis, A.W. Rosenbluth, M.N. Rosenbluth, A.H. Teller, E. Teller, J. Phys. Chem. A **21**, 1087 (1953).
22. S. Labidi, R. Masrour, A. Jabar, M. Ellouz, J. Magn. Magn. Mater. **523**, 167594 (2021).
23. F. Patterson, C.W. Moeller, R. Ward, Inorg. Chem. **2**, 196 (1963).
24. D. Sanchez, J.A. Alonso, M. Garcia-Hernandez, M.J. Martinez-Lope, J.L. Martinez, A. Mellergard, Phys. Rev. B **65**, 104426 (2002).
25. Y.A. Farzin, A. Babaei, A. Ataie, Ceram. Int. **46**, 16867 (2020).
26. Y. Konishi, H. Tokoro, M. Nishino, S. Miyashita, Phys. Rev. Lett. **100**, 067206 (2008).
27. E. König, Struct. Bond. **76**, 51 (1991).
28. N. Hachem, M. Alehyane, A. Lafhal, H. Zahir, M. Madani, A. Alrajhi, M. El Bouziani, Phys. Scr. **94**, 025804 (2019).
29. A. El Antari, H. Zahir, A. Hasnaoui, N. Hachem, A. Alrajhi, M. Madani, M. El Bouziani, Int. J. Theor. Phys. **57**, 2330 (2018).
30. B. Deviren, M. Keskin, O. Canko, Physica A **388**, 1835 (2009).

31. M. Karimou, R.A. Yessoufou, T.D. Oke, A. Kpadonou, F. Hontinfinde, Condens. Matter Phys. **19**, 33003 (2016).
32. J.M. Michalik, J.M. De Teresa, J. Blasco, P.A. Algarabel, M.R. Ibarra, C. Kapusta, U. Zeitler, J. Phys.: Condens. Matter **19**, 506206 (2007).
33. F.P. Sari, L.H. Suriasugandha, N. Franata, D. Handoko, IOP Conf. Ser.: Mater. Sci. Eng. **763**, 012071 (2020).